High resolution, non-contact surface metrology for freeform optics in digital immersive displays

Alex Sohn[a], Nelson Cardenas[a], Neil Naples[b],
Xavier Colonna de Lega[c], Jan Liesener[c], Thomas Dresel[c], Peter de Groot[c]

[a]Reality Labs, Meta, 9845 Willows Rd. Redmond, WA 9817
[b]Precitech, Inc., 44 Black Brook Rd, Keene, NH 03431
[c]Zygo Corporation, Laurel Brook Road, Middlefield, CT 06455

ABSTRACT

Freeform optical surface shapes have evolved from an intriguing optical design concept to a practical necessity for applications ranging from space and defense to consumer electronics. The demand for freeform solutions is no more strongly felt than in the development of digital immersive displays for augmented and mixed reality, where the combination of exceptionally high performance combines with ergonomic constraints of wearable interactive technologies. Some of these advanced designs call for diffraction-limited performance at large fields of view in off-axis orientations, often through conformal surfaces. Freeform optics are often the only way to correct the resultant aberrations, but their manufacture demands high-precision, high resolution surface figure metrology data such as can be obtained using coherence scanning interferometric microstitching (CSIM).

Keywords: Freeform, Interferometry, interferometer, metrology, topography, optical testing

1. INTRODUCTION

Freeform optical surfaces present multiple challenges through design, fabrication, and optical testing [1]. Developers consistently highlight the need for high accuracy surface metrology with high data density to reveal not only surface form, but fabrication fingerprints such as diamond turning marks. Surface metrology is essential not only for surface verification but also for closed-loop corrective polishing and machining. Currently a range of known methods are in place, including traditional mechanical contact profiling and computer-generated null correctors for interferometric testing. This leaves a critical need for flexible and agile measurement technologies that provide detailed topography information during development and production of complicated surface shapes characteristic of the latest optical design solutions.

What follows is and assessment of the freeform optics metrology landscape from a device point of view followed by the introduction of a new concept in surface figure metrology. Recent years have seen the emergence of more and more tools suitable for 3D figure metrology of freeform optical surfaces. These can be broadly classified into four groups: Profilometry, interferometry, deflectometry and sub-aperture stitching. By no means and exhaustive listing, addressed here are some relevant examples.

1.1 Profilometry

Profilometry typically involves single point scanning whether tracing on a curve or more complex geometry. Profilometers can be contacting or non-contact with a wide variety of sensors that can be applied to the method. 3D profilometry often relies on a precision motion system which can be programmed to trace complex surfaces and acquire data either point-to-point or in a scanning mode. Many configurations exist, from scanning probe microscopes (atomic force microscope, scanning tunnelling microscope) which, actuated piezoelectrically, can rapidly scan a very small area (typically 50 µm x 50 µm or less) with a variety of sensors to coordinate measuring machines (CMM's) that can scan surfaces of a square meter or more using tactile or optical sensors [2]. While contacting optical surfaces is generally undesirable, the most widespread systems used for measuring consumer level aspheric and freeform optics rely on tactile probing. Stylus profilometers, traditionally limited to 2D scanning can be found in 3D systems using rotary or translation tables and have used everything from LVDT to interferometric sensors. Reducing probing forces further, some systems use atomic force-based sensors and extremely sophisticated interferometric metrology frames made of low-expansion ceramics to achieve measurement uncertainties well below 100 nm [3]. Generally, contact profilometry is limited by the physical inertia of the sensor as this produces errors due to mechanical deflection of the surface or the sensing system. Minimizing these errors often requires low accelerations which then translates into long acquisition times or relatively low data density.

Polar-based 3D profilometers [4,5] mitigate the impact of motion path accelerations by rotating the sample to avoid acceleration reversals associated with rastering. The advantages of these rotational systems diminish as non-rotationally symmetric departure increases in the measurement since a linear probe axis must then experience increasing accelerations due to reversals even when the main scanning axes do not. Additionally, rotational systems are highly dependent on the alignment accuracy of the sensor relative to the rotational axis. This requires frequent calibration and in-process compensations.

Finally, no listing of profilometry systems would be complete without mentioning *in-situ* metrology systems. These are often linear sensors installed on diamond turning machines (DTM's) that use the precision motion axes of the machine to position the sensor for measurement. Sensors vary from CMM touch probes to air-bearing LVDT* sensors to chromatic confocal (CA). One such in-situ system was used in measurements presented here. It consists of a 5-axis diamond turning machine (XYZCB) and a 300 μm range CA sensor. The advantage of multi-axis motion in this system is that multiple surfaces, including datums and functional surfaces, can be measured in the same coordinate system, allowing for the accurate establishment of the relative positions in space. While simple in concept, in-situ systems – particularly with rotary axes – require careful alignment, compensation for geometric axis errors and probe errors. The latter are particularly important in CA probes due to the probes' inherent angle-of-incidence errors [6]. With such alignment and compensation, these systems can be relied upon for uncertainties well below 1 μm.

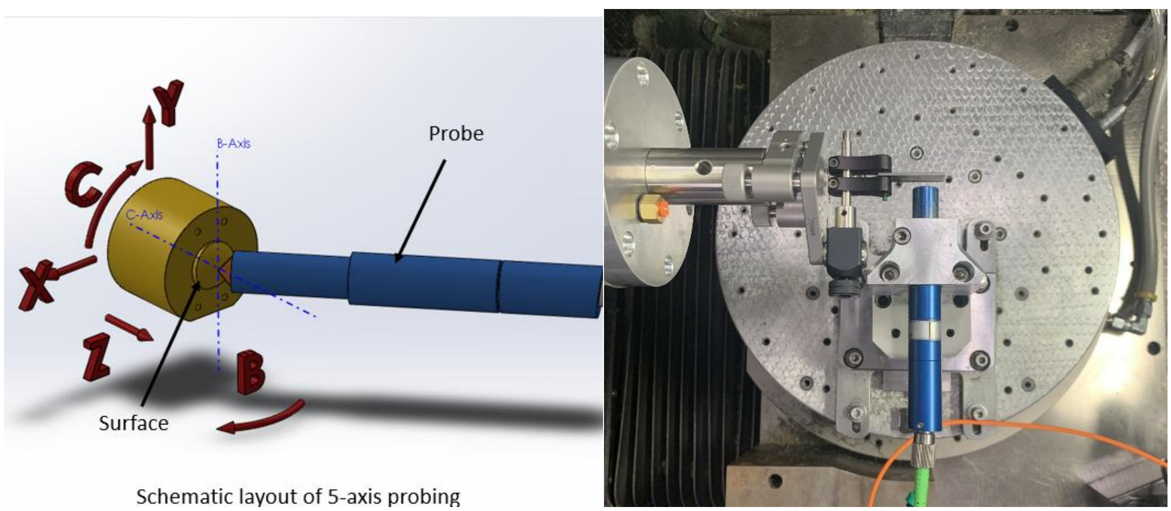

Figure 1. In-situ metrology system consisting of a 5-axis diamond turning machine populated with a chromatic confocal sensor for gathering surface data. As shown, the system is probing a gauge block for probe alignment.

When weighing the advantages and limitations of profilometry systems, it is important to note that the flexibility of many of these systems is generally unmatched by other measurement techniques and they are the go-to when uncertainties and departures are large.

1.2 Interferometry

A mature area of interferometry that has found applications in freeform optics is CGH (Computer Generated Hologram) interferometry. This is a highly case-specific custom solution for measuring freeform optics [7]. Each surface prescription requires a unique CGH, which must be individually designed and fabricated, typically using e-beam lithography, at significant cost. Additionally, low-order aberrations and prescription information (power, spherical aberration, astigmatism and coma) are not inherently presented via CGH metrology but must be derived from alignment data. However, the latter can be integrated into the CGH itself [8] though tolerancing of datums and fiducials directly impacts SFE of prescription components. Furthermore, alignment can be challenging due to a small error envelope. However, this has been addressed in large part by intelligent alignment fiducial design and as shown in Figure 2, it is sometimes difficult to exclude unwanted diffraction orders from the measurement surface in the design. Finally, CGH's are intolerant of large form errors since high fringe densities associated with significant slope departure will prevent the reconstruction of a complete phase map. Given these considerations, however, CGH interferometry can deliver high-throughput and large area surface mapping particularly suited to well-controlled surfaces with minimal departures. In a production environment, the short cycle times in particular place CGH metrology in a class by itself when it comes to measuring many samples.

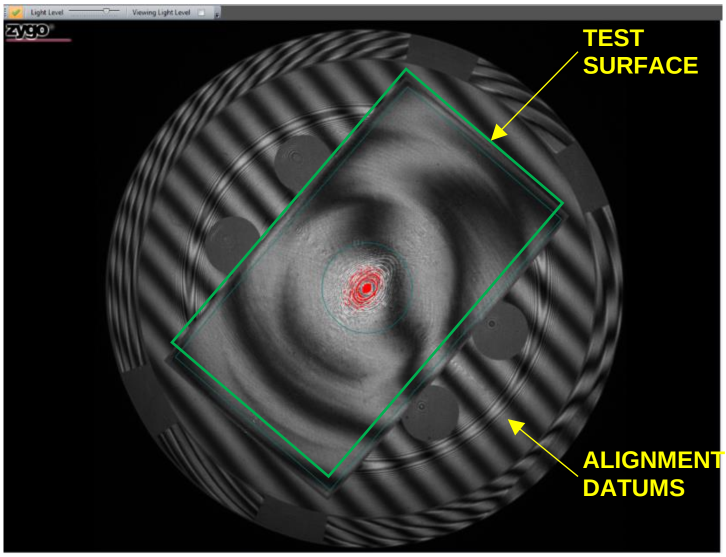

Figure 2. CGH interferogram showing rectangular test surface, multiple datum and alignment surfaces, and zero-order interference (in red) at the center of the measurement area. This center must be masked for measurement and represents some loss of data. The image shows the first case study measurement described in the text.

Other forms of interferometry have also recently been brought to viability for free-form optics. Of particular note is the tilted-wave interferometer [9], which has shown promise on surfaces with relatively mild free-form departures, though future development may see wider application.

1.3 Deflectometry

Various deflectometry techniques exist (Schack-Hartman testing, single-point, line scan, fringe projection) but the most relevant to freeform surface metrology is phase measuring deflectometry [10]. In this method, a fringe pattern typically generated on a flat panel is imaged in reflection off a test surface. The perturbation of this fringe pattern or set of fringe patterns can then be used to calculate the surface slopes and, consequently the profile of the test surface. The method can be broadly applied to a wide range of surface geometries, requires relatively low-cost hardware and is very fast in data acquisition. However, the method has not been widely employed to date because it is application-specific and requires a custom test design, sensitivity analysis and phase retrieval algorithm as well as careful calibration. Additionally, may geometries are unsuitable for this type of testing (strong convex prescriptions, for example) and the needed measurement resolution cannot be achieved.

1.4 Sub-aperture stitching

Stitching interferometry has been used for large surfaces [11], flat areas requiring high data density [12], aspheres [13] and increasingly, free form surfaces [14]. It is an extension of phase shifting interferometry (PSI) where multiple, overlapping sub-apertures combine with data from positioning systems to reconstruct a larger surface measurement than would be possible with a single data acquisition. Reference objectives must be chosen carefully, and the stitching plan carefully designed so as not to exceed the slope range of the measurement system, which is typically small on a single-frequency PSI. Computational methods for reducing accumulation of stitching and retrace errors have greatly extended the application range of these systems of late, though they can be defined as still operating in the range of relatively small departure from a nominal spherical or flat profile.

2. METROLOGY PROCESS DESCRIPTION

High-resolution coherence scanning interferometric microstitching (CSIM) is a new method for robust surface figure measurements on asymmetric freeform optics [15]. The measurement principle relies on integration of detailed 3D images acquired over a sequence of part orientations. Unlike many conventional stitching solutions that rely on a rigid metrology frame, our approach leverages the micro roughness present even in highly polished surfaces to register the 3D images to each other. In this way, we avoid the requirements and limitations of ultraprecision motion axes. Inventive methods for precise calibration and traceability of the individual 3D images, including *in-situ* interferometric scaling of the measurement axes as well as compensation for slope-dependent errors, enables accurate results on even the most complex surface shapes.

The high data density and lateral resolution provide a broad spatial frequency spectrum for the measured topography, containing roughness data, mid-spatial frequency information and microstructure data. As an example, we show in Fig. 3 a test sample for a complex freeform hierarchical surface comprised of an array of concave freeform lenslets, tilted and superimposed onto a convex freeform base surface. This is a generalized surface with no optical prescription *per se*, yet accessible to an interferometric measurement based on our interferometric metrology solution, illustrating the capabilities and potential of the approach.

The development of this new surface metrology concept was initially driven by the unmet need for measuring the full surface of small lenses and lens molds for cell phone cameras. Besides being small (2 to 8 mm in diameter) and rotationally symmetric, these lenses show an unprecedented range of surface slopes (up to 80 degrees) and profiles (including gullwing and pancake shapes). Because of the dimensions of these lenses and molds, as well as the frequent need to inspect their surface roughness, 3D Interference microscopy provided a suitable platform to start investigating solutions for this challenging metrology task [16]. Many of these lenses show strong local slope and curvature variations that require at least 10X or 20X objectives to capture the local surface topography with an interference microscope. The choice of such objectives is driven by the need to capture the specular light that reflects from the sample surface, enabled by the numerical aperture ranges available at these magnifications. The corresponding fields of view, however, are typically restricted to sizes on the order of 1 mm. This implies that it is impossible to measure an entire surface of interest in a single data capture. A stitching approach, where overlapping "tiles" of data are captured sequentially over the entire surface can, in theory, provide the required measurement flexibility. Such techniques often rely on combining topography data with position information derived from a metrology frame, such as encoded motion axes. The technique described here relies instead on the self-consistency of the topography data, eliminating the need for an accurate metrology frame. The tradeoff is that this places more demanding requirements on the in-position stability of the metrology platform. To this end, a 5-axis motion system was developed to provide the navigation flexibility required to handle the broadest possible range of surface shapes.

Early development revealed that several issues needed to be addressed to successfully stich an entire cell phone camera lens surface. The first step was to develop a full three-dimensional stitching algorithm capable of shifting and rotating each tile using 5 or 6 degrees of freedom. All the relative rigid body motions between tiles are optimized by the stitching algorithm simultaneously, whereby the first (usually the central) tile provides an anchor around which all other tiles are placed. While initial experiments were very encouraging, they revealed discrepancies in the regions of tile overlap that stemmed from aberrations in the imaging optics. These aberrations can be separated into two categories: first, imaging distortions that affect the mapping of the periodic camera pixel array onto corresponding lateral coordinates in sample space. This effect can be characterized and compensated by measuring and analyzing a high accuracy lateral calibration standard. The standard used in this case is a periodic pattern of square raised features manufactured by VLSI. The 10-µm pitch of a master standard was characterized at the National Metrology Institute of Germany (PTB) with a measurement uncertainty of 0.0002 µm (k=2). This master standard is used to characterize derived calibration artifacts for which the pitch is determined with an uncertainty of 0.0005 µm (k=2). The second category of optical effects are so-called retrace errors, optical path differences which are due to the different optical paths that the reference and test beams take as they travel through the illumination and imaging optics of the interference microscope. We developed a calibration method to characterize retrace errors using a small calibration sphere which gives a surface patch that is considerably smaller than the field of view. By moving this sphere to various positions within the field of view, it is possible to collect information about retrace-induced deformation of the measured topography and how these deformations depend on the field of view. This results in a four-dimensional calibration polynomial which describes the retrace errors as a function of (x, y) and chief ray slope coordinates (or surface slopes) (u, v). This 4D-function is then used to correct every topography tile for retrace errors – after it has been corrected for distortion. Concave BK7 spheres with a nominal radius of curvature of 0.5 mm are used for this calibration. The absolute deviation from perfect sphere is characterized as part of the calibration procedure by automatic application of an N-shear reversal algorithm. The nominal radius of curvature of each calibration sphere is derived from a comparison to a master sphere that was characterized on the micro-CMM developed at the Swiss Federal Institute of Metrology (METAS) [17]. The uncertainty of measurement for the roundness and diameter of the master sphere are 0.03 µm and 0.05 µm (k=2), respectively.

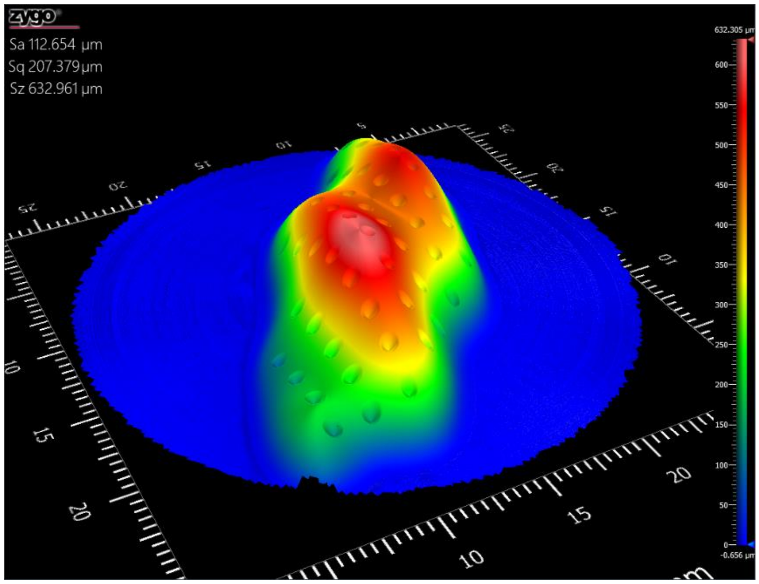

Figure 3: Freeform microlens array measured via coherence scanning interferometric microstitching (CSIM). The technique allows the measurement of surfaces with departures of several millimeters from a nominal planar or rotationally symmetric design with relatively large slopes.

Another possible contribution to measurement uncertainty for this stitching application is the nominal amplification and non-linearity of the piezo-driven stage used to scan the interferometric objective through the measurement volume. The instrument automatically performs periodic self-calibrations of the stage non-linearity by measuring the rate of phase change per captured camera frame when measuring a nulled reference mirror embedded in a calibration shelf. The overall scale (or average velocity) of the scan is derived from the knowledge of the center wavelength of a 3-nm narrowband filter used during this procedure. The filter center wavelength is factory-calibrated using a spectrophotometer and a reference HgAr arc lamp [18].

With the calibrations and corrections in place, we observe nm-level agreement between stitched tiles. For example, Fig. 4 shows a diagnostic map generated when stitching 77 tiles to reconstruct a sub-region of a 1-mm diameter sphere. The nominal overlap fraction is 50% between neighboring tiles. Each map value represents the standard deviation of the overlapping tiles combined at that location to generate the final stitched map. The maximum standard deviation is less than 5 nm in this example. The average standard deviation is less than 2 nm, illustrating the high level of agreement between individual tiles.

The agreement in the overlapping regions between neighboring tiles can be decomposed into two components: the agreement of the local form and the agreement of the surface roughness. In the ideal case, both components lock the tiles together simultaneously. In cases where the rigid body motions of the form would be ambiguous (such as the stitching of flats, cylinders, or spheres), it is the roughness terms which lock the tiles together unambiguously. This points to a key enabling element of this metrology technique: the ability of interference microscopy to resolve nm-level surface roughness with sub-nm measurement noise at spatial frequencies in the many hundreds of cycles per mm. Early experiments confirmed that even super-polished glass surfaces exhibit clearly resolvable surface finish patterns that provide unequivocal information for repositioning overlapping topography maps. Figure 5 shows a 40-µm patch of topography data measured on an uncoated BK7 lens with 0.4-µm lateral sampling. The cross-correlation peak computed between two similar patches measured near a common location provides information about the relative lateral position of the two patches. The 1-σ repeatability of the peak position is 0.018 µm in this example. In other words, an algorithm based on surface finish correlation can realign two tiles of data with a lateral noise lower than one twentieth of a pixel.

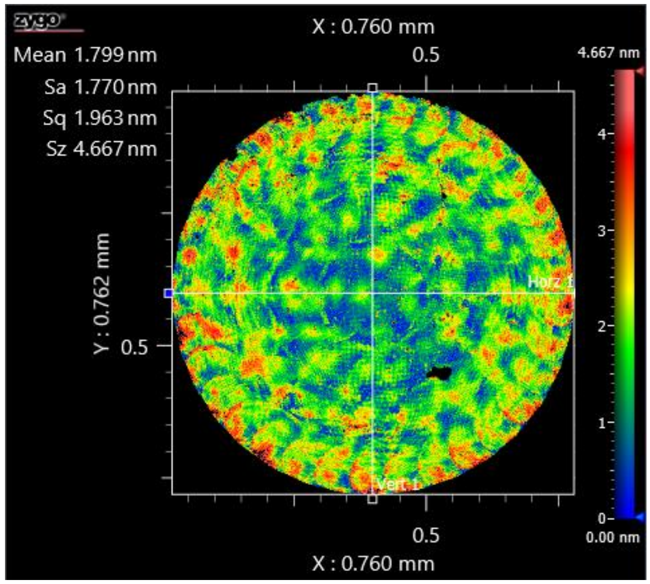

Figure 4. Map of standard deviation of overlapping tiles in a 77-tile stitch of a 1-mm diameter sphere. See text for details.

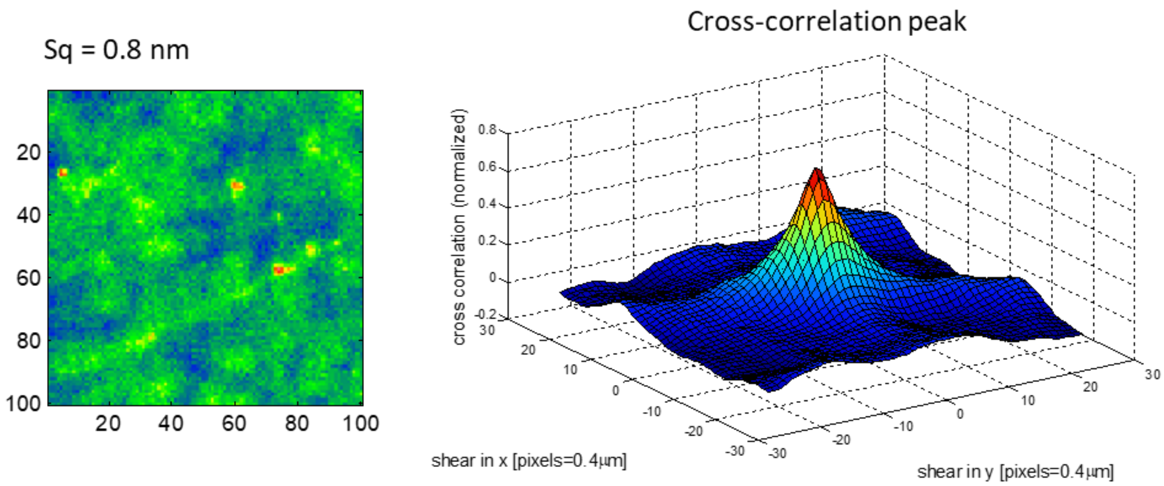

Figure 5 (a) 40 µm x 40 µm topography data measured on off-the-shelf uncoated BK7 lens. Surface RMS is 0.8 nm. (b) Cross-correlation peak of surface data computed for two 40 µm x 40 µm patches collected at the same nominal location on the lens.

For rotationally symmetric aspheres, the metrology software supports two measurement modes: first, a prescription mode where the user provides the optical design of the surface under test and the software then drives the 5-axis stage system of the instrument to pre-computed locations on the surface to collect the tiles. Second, a so-called “follower” mode where the instrument starts with the central tile and then predicts the expected stage positions to collect neighboring tiles by applying surface and surface-derivative continuity arguments. This second mode does not need the input of a prescription, which makes it possible to measure unknown surface shapes.

We took this idea one step further by developing a “freeform follower mode.” This acquisition mode does not assume that the surface is rotationally symmetric. It again starts with the central tile and then finds several continuation points within the surface patch it just measured. Following the idea of a flood fill algorithm frequently used in image processing, the instrument then proceeds by pushing these continuation points into a priority queue. It then pulls out the following positions from this queue and walks to the new location. Internally, it keeps track of the coverage provided by the collected tiles in a three-dimensional space. The user selects one or more exit criteria to limit the search for new tiles. For instance, this is required to make sure that the software does not continue with neighboring surfaces on the test part which are not of interest for the freeform surface itself. Exit criteria include slope or curvature continuity. This new measurement mode is the most flexible: the user can start from any position on the surface of interest, and the instrument can proceed automatically without needing any further pre-alignment of the test part, which makes this mode very easy to use and reduces part setup time.

3. CASE STUDIES

To demonstrate the capabilities of CSIM, two case studies are presented: a biconic reflector used as a collimating component in a projector system, and a complex freeform that includes an arbitrary surface populated by a microlens array. Due to its resemblance to certain protists, this latter surface has been nicknamed "The Amoeba".

3.1 Biconic Mirror

Fig. 6 shows the biconic mirror consisting of an optical surface, a datum flat and four alignment spheres. The component was designed to allow datuming and alignment in multiple metrology and test setups. The surfaces were diamond turned using fast tool servo technology in RSP aluminum.

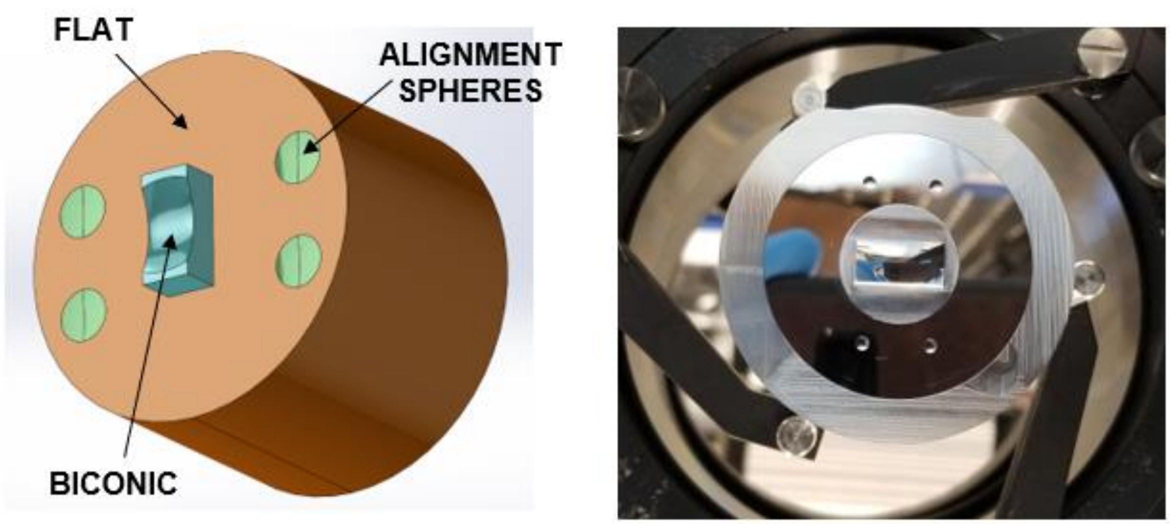

Figure 6. Diamond-turned biconic freeform consisting of an optical surface, a datum flat and four alignment spheres. The actual part is show at right in aluminum.

The prescription of the biconic ellipsoid is as follows

$$z = \frac{C_x x^2 + C_y y^2}{1+\sqrt{1-(1+k_x)C_x^2 x^2-(1+k_y)C_y^2 y^2}} + A_r\left\{\left(1-A_p\right)x^2 + (1+A_p)y^2\right\}^2, \qquad (1)$$

Where C_x=-0.0794 and C_y=0.0156 are the curvatures in the x- and y- directions, $k_x = k_y = 0$ are the conic constants and A_r=-0.00118 and A_p=0.290 are the biconic coefficients used to calculate the surface profile.

3.2 Complex Hierarchical Freeform "Amoeba"

To demonstrate complex surface data acquisition and more qualitative analysis and related surface processing tools, the hierarchical surface shown in Fig. 7 was conceived. This surface consists of an array of concave freeform lenslets, tilted and superimposed onto a convex freeform base surface. Designed to be machinable using established diamond turning techniques and measurable on multiple free-form metrology platforms, this surface owes its complexity to an overall asymmetry, individual lenslet tilts, non-circular boundaries, and high continuity blends. More importantly, it is a surface with no optical prescription *per se* and most practical optical designs represent a limiting case of this general example. The explicit lenslet and base surface prescriptions before any translations or coordinate frame transformations are respectively given as

$$Z_L(X,Y) = -\frac{14}{25}\left(\sqrt{20\sqrt{100-Y^2}-Y^2-5X^2+61}+4\cos\left(\frac{\sqrt{X^2+Y^2}}{2}\right)-\frac{11241}{560}\right) \tag{2}$$

$$Z_B(X,Y) = \frac{2}{25}\left(\frac{X}{5}\left(Y+\frac{3}{2}\right)-\sin(X)-\frac{(Y+1)^2}{10}-\frac{X^2}{5}-\frac{\sin(Y+1)}{4}+\frac{23}{4}\right) \tag{3}$$

All 54 concave lenslets are individually tilted about the X and then Y-axis such that they are normal to the base surface at their respective locations. The sag of each lenslet and the base surface are 46 µm and 633 µm, respectively. The base surface boundary is equal to its intersection with the Z=0 plane and the overall surface boundary is circular. All lenslet boundaries are unique, non-circular, and equal to the 3D intersection curve between each lenslet and the base surface. As designed, the maximum azimuthal slope of the entire surface is 22.8°, and the overall range of radial slopes is 38.8°. Therefore, it is possible to machine this surface with any common diamond machining process such as XZC-turning or XYZ-milling.

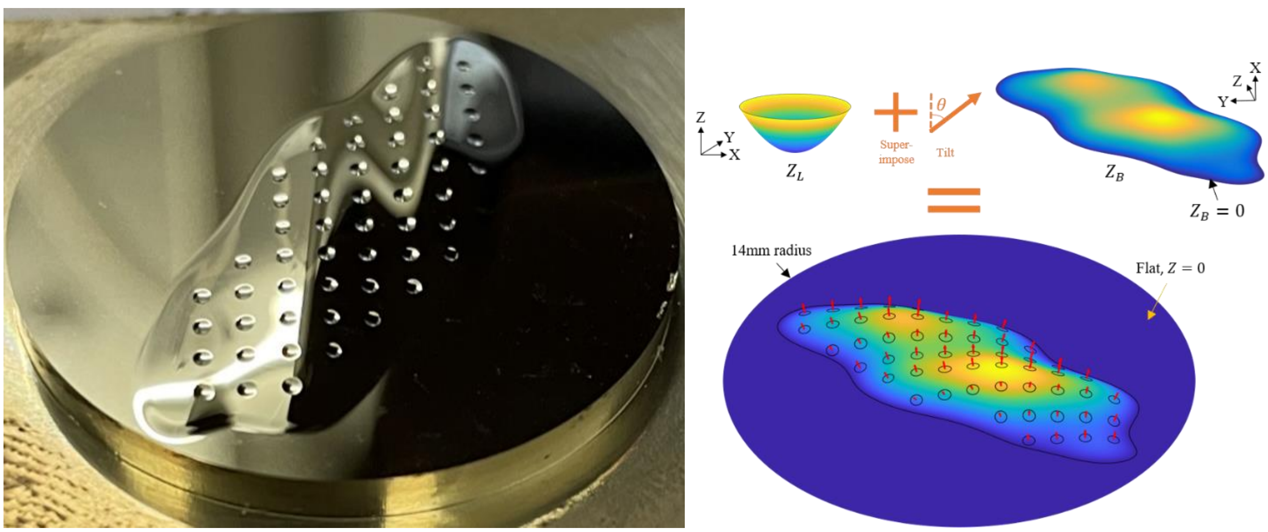

Figure 7. Freeform "Amoeba". Lenslet normal directions shown in red. The designed surface is C^0 continuous. After blending, the machined surface is C^3continuous.

4. MEASUREMENT RESULTS

4.1 Biconic Mirror Measurements

Measurements of the Biconic mirror were performed using in-situ chromatic confocal scanning described in section 1.1 and using CSIM. In-situ data was imported and gridded in Zygo Mx software and fit to prescription data imported from CodeV and ZEMAX optical design files. The measurement results for each method, shown in Figs. 8 and 9, respectively correlate well near the center of the clear aperture with comparable Sz and Sq values. At the very edge of the in-situ data, the error diverges sharply, most likely due to the steep slope of the surface (28°) where angle-of-incidence error correction becomes less accurate.

Such measurement errors not only drive the error map but can also distort it by skewing the fit. One way to circumvent this would be to rotate the probe closer to a surface normal direction, but this would, in turn, contribute alignment errors to the results. The CSIM measurement does not show such a departure near the edge, instead illustrating a much more compliant surface away from the center.

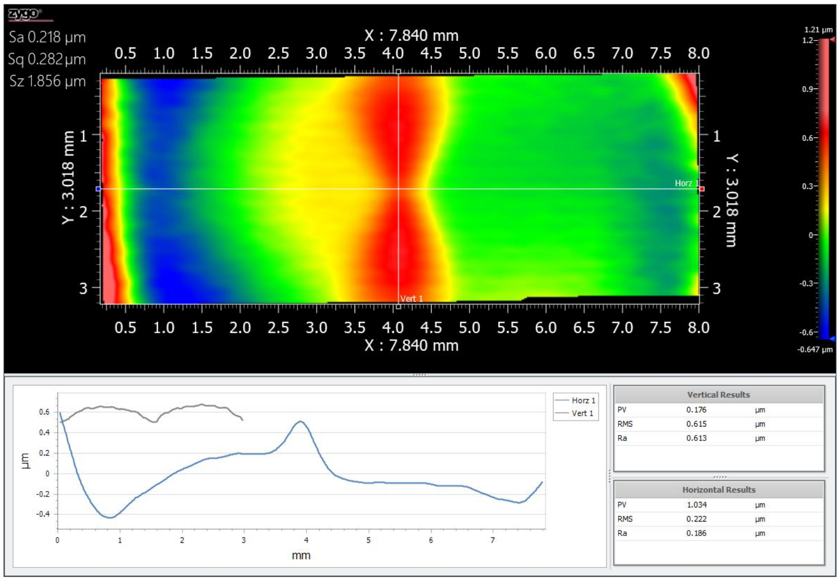

Figure 8. In-situ chromatic confocal probe measurement residuals are shown. When compared to the CSIM measurement, while the Sz (PV) and Sq values are comparable, particularly when considering the occlusion and smaller aperture of the former, the center "Bowtie" feature is clearly visible.

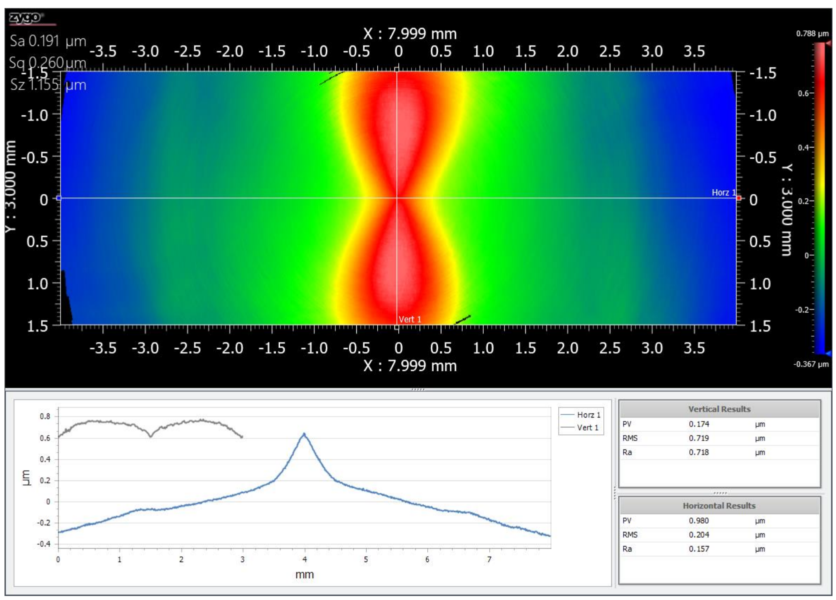

Figure 9. Stitching results for the CSIM method. Sz and Sq parameters are comparable to those of the in-situ measurement and the central "Bowtie" feature is a distinctive feature of both measurement results.

4.2 Amoeba Measurements

The "Amoeba" hierarchical free-form surface has been measured using both the in-situ chromatic confocal system and CSIM. Measurement with the in-situ platform collected approximately 6.5 million data points while the CSIM system collected about 200 million data points to create a high-resolution surface profile map. This measured data was compared to the prescription and the two data sets to each other using best fits.

Figure 10 compares the amoeba surface measured with both the chromatic confocal probe and CSIM to the surface prescription. To generate the left plot, the 3D point cloud measured on the diamond-turning machine is interpolated and resampled to a square grid. A least-square fit then optimizes six rigid body motions to minimize the RMS distance between the measured data and the surface prescription, and the plots show the residual distance between the two surfaces after alignment. The RMS (Sq) difference in the in-situ data is 0.35 µm and the RMS difference for the CSIM data is 0.43 µm. The height difference in most of the lenslet regions looks like linear gradients, suggesting a lateral misalignment of the lenslets between design and physical sample.

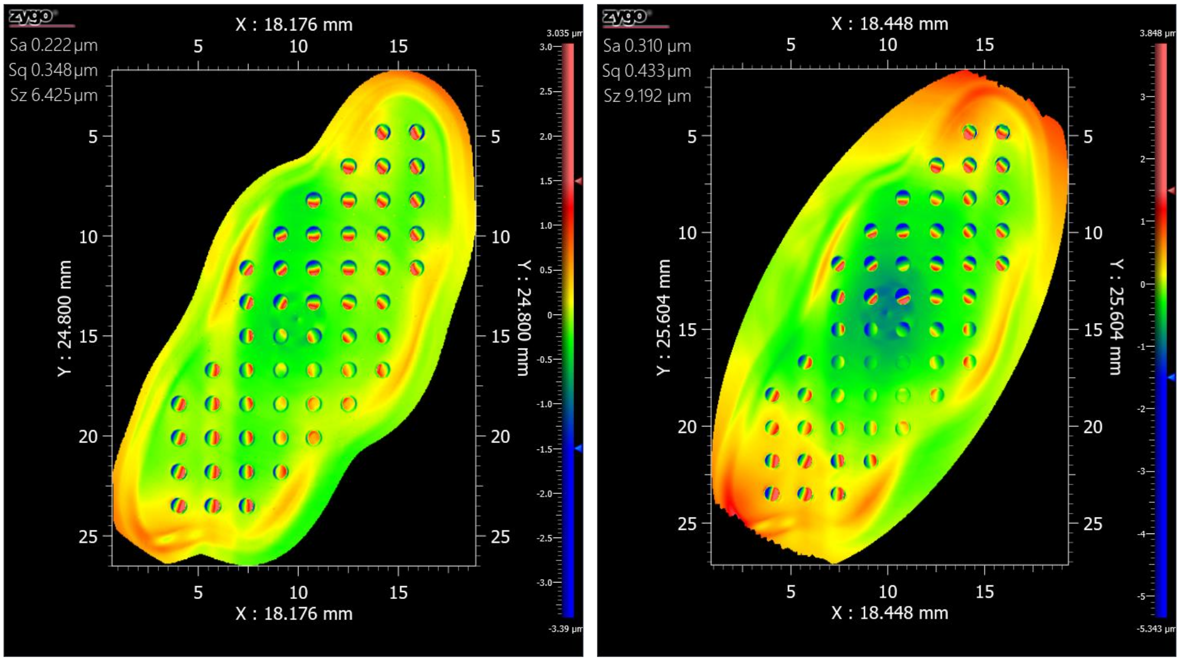

Figure 10. Difference between topography map derived from chromatic confocal sensor data and prescription after rigid body alignment (left), and difference between the microstitched topography map and prescription after rigid body alignment (right). Color scale range is -1.5 µm to 1.5 µm for both plots.

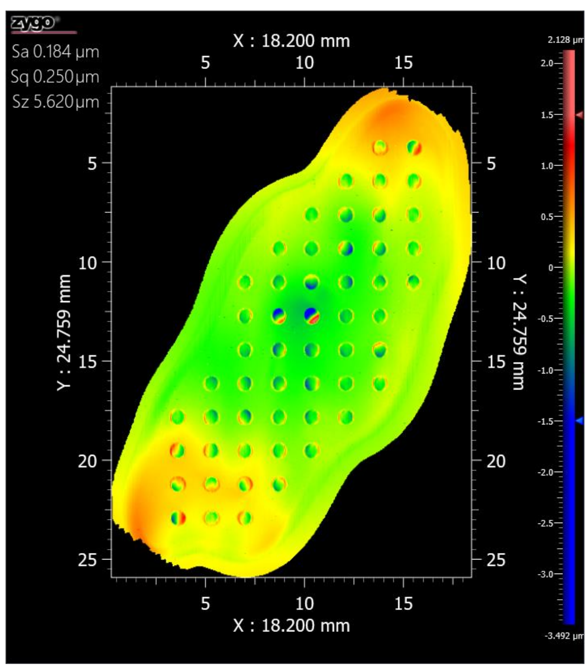

Figure 11. Difference between topography map derived from chromatic confocal sensor data and microstitched measurement, after rigid body alignment. Color scale range is -1.5 µm to 1.5 µm.

The plot of Figure 11 shows the difference between the chromatic confocal and CSIM data after rigid body motions minimization. The RMS difference is 0.25 µm, showing a better agreement between the two measurement results than between each measured surface and the prescription. Note that, except for two lenslets near the center, most of the linear gradients observed previously in the lenslet regions are eliminated or reduced. The gradients at these two locations can be traced back to misalignments in the microstitched data and uncompensated angle-of-incidence data from high slope regions. Additionally, the edge effects from fitting data sets with irregular aperture can skew fit convergence and reduce the quality of the fit. Customized fitting algorithms beyond least-squares and robust datuming could potentially improve fit quality if standard deviations in the correlation residual of better than 0.25 µm are required, though we can conclude that, were the measured data of either measurement method used to compensate the shape errors, the result would have a similar uncertainty.

5. CONCLUSIONS

While the array of available technologies and sensors for measuring surface figure in free-form optics is growing, coherent scanning interferometric microstitching (CSIM) has been demonstrated to provide high resolution, high-accuracy surface metrology data over a wide spatial frequency spectrum. The high vertical (~1Å) and lateral (1 µm) resolution enables characterization from surface figure to mid-spatial errors and surface roughness in one measurement. Using the surface itself for motion feedback makes executing the measurement simple from a user standpoint and could be used for reconstructing (reverse-engineering) unknown profiles. And all of this has been demonstrated on complex free-form surfaces with high surface slopes and departures from rotational symmetry that are extremely challenging to measure by other means. Agreement with chromatic confocal probe in-situ metrology has been demonstrated to a standard deviation of 0.25 µm, making it a versatile and capable tool for measuring free-form optical surfaces.

REFERENCES

1. Rolland, J. P., Davies, M. A., Suleski, T. J. et al., “Freeform optics for imaging,” Optica 8(2), 161-176 (2021).
2. Cole, G. C., Garfield, R., Peters, T. et al., "Optical Fabrication of the James Webb Space Telescope Primary Mirror," OSA Technical Digest (CD), OFMA2 (2006)
3. Shiozawa, H., Fukutomi, Y., Ushioda, T. et al., "Development of ultra-precision 3D-CMM based on 3-D metrology frame," Proc. ASPE 18, 15-18 (2018).
4. Berger, G., and Petter, J., “Novel technology for high precision, fast non-contact asphere metrology,” Technisches Messen 81(1), 2-7 (2014).
5. Sohn, A., K., G., and Dow, T., "The spherical profilometer Polaris 3D," Proc. ASPE 47, 43-46 (2009).
6. Nouira, H., El-Hayek, N., Yuan, X. et al., “Characterization of the main error sources of chromatic confocal probes for dimensional measurement,” Measurement Science and Technology 25(4), 044011 (2014).
7. Sohn, A., Garrard, K., Ohl, R. et al., " Figure Metrology of a Free-Form Optical Surface," Proc. ASPE (2002).
8. Zhao, C., "Computer-generated hologram for optical testing: a review," Proc. SPIE 11813, 118130K (2021).
9. Pruss, C., Reichelt, S., Tiziani, H. et al., “Computer-generated holograms in interferometric testing,” Optical Engineering 43(11), (2004).
10. Huang, L., Idir, M., Zuo, C. et al., “Review of phase measuring deflectometry,” Optics and Lasers in Engineering 107, 247-257 (2018).
11. Bray, M., "Stitching interferometry: how and why it works," Proc. SPIE 3739 (1999).
12 DiSciacca, J., Pultar, R., Colonna de Lega, X. et al., "Interferometric measurements of mold-plate assemblies designed for high-volume manufacturing of aspheric microlenses," Proc. SPIE 11352, 113520M (2020).
13. Tricard, M., Kulawiec, A., Bauer, M. et al., " Subaperture stitching interferometry of high-departure aspheres by incorporating a variable optical null," Proc. CIRP Annals 59, 547-550 (2010).
14. Hovis, C. (2019). “Optical metrology of freeform optics utilizing interferometric stitching”. Unc Charlotte Electronic Theses and Dissertations
15. Colonna de Lega, X., Dresel, T., Liesener, J. et al., "Optical form and relational metrology of aspheric micro optics," Proc. ASPE 67, 20-23 (2017
16. de Groot, P., “Principles of interference microscopy for the measurement of surface topography,” Advances in Optics and Photonics 7(1), 1-65 (2015).

17. Küng, A., Meli, F., and Thalmann, R., “Ultraprecision micro-CMM using a low force 3D touch probe,” Meas. Sci. Technol. 18, 319 (2007).
18. de Groot, P., and Beverage, J., "Calibration of the amplification coefficient in interference microscopy by means of a wavelength standard," Proc. SPIE 9526, 952610.1-52610.11 (2015).